JACS
JOURNAL OF THE AMERICAN CHEMICAL SOCIETY

Article

pubs.acs.org/JACS

Self-Assembled Nanoscale DNA–Porphyrin Complex for Artificial Light Harvesting

Jakob G. Woller, Jonas K. Hannestad, and Bo Albinsson*

Department of Chemical and Biological Engineering/Physical Chemistry, Chalmers University of Technology, S-41296 Gothenburg, Sweden

Supporting Information

ABSTRACT: Mimicking green plants' and bacteria's extraordinary ability to absorb a vast number of photons and harness their energy is a longstanding goal in artificial photosynthesis. Resonance energy transfer among donor dyes has been shown to play a crucial role on the overall transfer of energy in the natural systems. Here, we present artificial, self-assembled, light-harvesting complexes consisting of DNA scaffolds, intercalated YO-PRO-1 (YO) donor dyes and a porphyrin acceptor anchored to a lipid bilayer, conceptually mimicking the natural light-harvesting systems. A model system consisting of 39-mer duplex DNA in a linear wire configuration with the porphyrin attached in the middle of the wire is primarily investigated. Utilizing intercalated donor fluorophores to sensitize the excitation of the porphyrin acceptor, we obtain an effective absorption coefficient 12 times larger than for direct excitation of the porphyrin. On the basis of steady-state and time-resolved emission measurements and Markov chain simulations, we show that YO-to-YO resonance energy transfer substantially contributes to the overall flow of energy to the porphyrin. This increase is explained through energy migration along the wire allowing the excited state energy to transfer to positions closer to the porphyrin. The versatility of DNA as a structural material is demonstrated through the construction of a more complex, hexagonal, light-harvesting scaffold yielding further increase in the effective absorption coefficient. Our results show that, by using DNA as a scaffold, we are able to arrange chromophores on a nanometer scale and in this way facilitate the assembly of efficient light-harvesting systems.

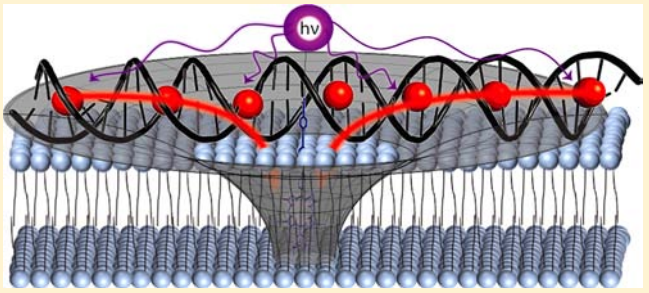

INTRODUCTION

The light-harvesting complexes of photosynthetic bacteria are remarkable examples of nanoscale architecture, comprising a series of chromophores providing a wide coverage of the solar spectrum and a spatial organization that ensures directional transfer of excitation energy to the reaction center.[1,2] Solar energy is efficiently absorbed by chlorophyll donor dyes, which are precisely positioned in ring-like, membrane-bound, protein complexes, then shuttled toward a single acceptor dye located in the reaction center via homo and hetero (resonance) energy transfer processes (FRET). The energy is used to create a charge-separated state which subsequently reduces a quinone to hydroquinone through electron transfer processes. Light-harvesting complexes serve two purposes by both increasing the region of the solar spectrum where absorption occurs and by increasing the rate at which the reaction center receives excitation energy, allowing a turnover which can be 2 orders of magnitude greater than what would be achieved by direct excitation of the reaction center. Such a marked increase in catalytic turnover has sparked a great deal of research in the field of artificial photosynthesis and light harvesting in particular, with goals of increasing throughput of catalytic reactions, as well as photonic applications.[3−6]

Many attempts have been made to mimic natural light-harvesting systems using complex organic molecules, capable of both energy- and electron-transfer processes.[7−12] These examples employed covalent bonds as the mode of structure formation yielding large hydrophobic molecules needing organic solvents. Only a few donor dyes per acceptor were included due to the difficulty of synthesis, as compared to the hundreds of donor dyes found in nature.[2] To increase the ratio of donor to acceptor dyes new synthesis pathways employing self-assembly and dendrimers have been investigated, however, without the ability to harness the harvested energy through electron transfer processes.[13−18]

DNA is a prime example of a self-assembled molecule, forming a duplex based solely on matching nucleobase sequences. The advent of DNA nanotechnology means that complex DNA structures are routinely available and can be designed.[19−21] DNA is a commonly used scaffold for positioning of chromophores.[22−26]

Here, we present a self-assembled mimic of photosynthetic light harvesting by employing duplex DNA as a nanoscale scaffold material able to position donor and acceptor

Received: December 4, 2012
Published: January 25, 2013

dx.doi.org/10.1021/ja311828v | J. Am. Chem. Soc. 2013, 135, 2759−2768

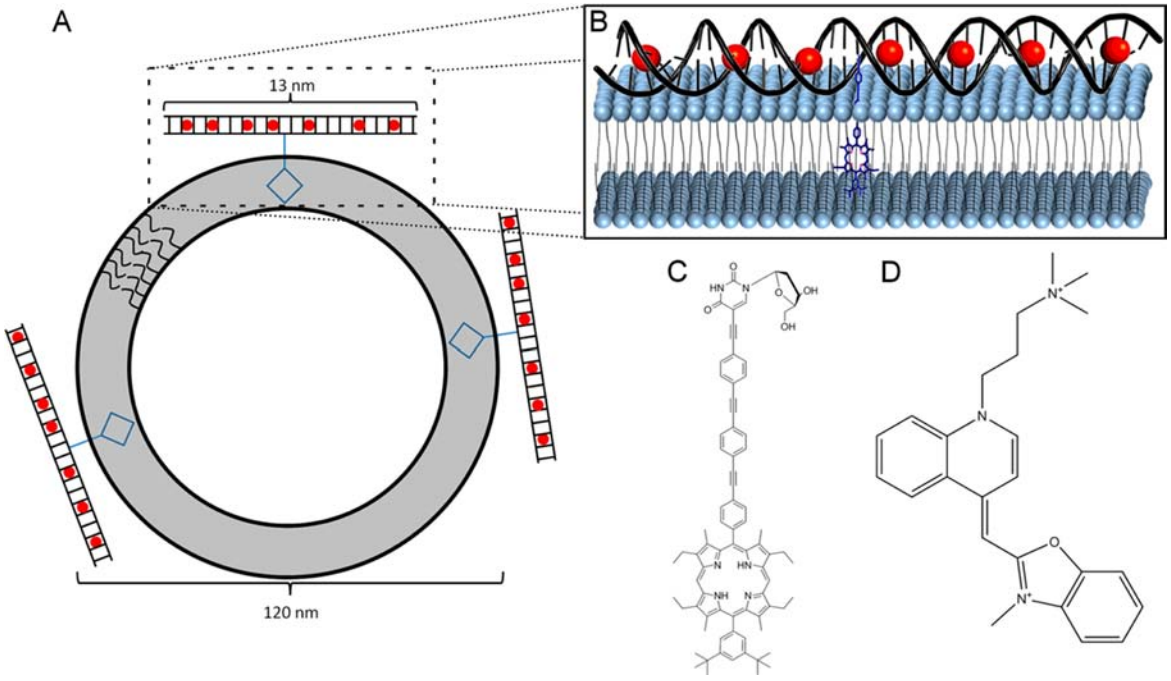

Figure 1. (A) Schematic figure of the YO−DNA−porphyrin system bound to lipid vesicles (not to scale). (B) A close-up showing a single DNA−porphyrin construct with seven intercalated YO molecules, bound to a vesicle bilayer via porphyrin. (C) Chemical structure of the porphyrin−thymine nucleoside (acceptor). (D) Chemical structure of YO-PRO-1 (YO) energy donor.

chromophores with base-pair (bp) precision, in an architecture reminiscent of the natural system. Aside from the DNA scaffold, the light-harvesting assembly has three main constituents. First, the intercalating dye YO-PRO-1 (YO) acts as an excitation energy donor. YO binds between DNA base-pairs (intercalates) with nearest neighbor exclusion, which will minimize contact quenching. When excited, the donors transfer excitation energy to the second constituent, a porphyrin acceptor which is also a quite potent reduction agent in its excited state, a necessary prerequisite for using the harnessed energy. The porphyrin acceptor is covalently attached to a thymine positioned in the middle of one strand of a 39-mer DNA duplex via a phenylethynylene linker (see Figure 1 for a schematic diagram of the system). In addition to being an excitation energy acceptor and potential redox site, the porphyrin moiety also anchors the complex to a liposome (the final constituent), creating a biphasic system with DNA in the aqueous phase and porphyrin in the lipid phase.

The final structure is completely self-assembled and formed by simple mixing of the constituent parts. This modularity allows easy substitution to other intercalating dyes, modified DNA strands, or novel lipids. The inherent ability to vary the concentration of donor dyes per porphyrin acceptor allows a unique opportunity to study the effects of homo-FRET in a light-harvesting system, since this depends on the average dye-to-dye distance. When the system is saturated with donor chromophores, the YO-to-YO distance will be ∼10 Å, taking into account unwinding of the helix upon intercalation, yielding a donor spacing which is comparable to the ∼9 Å spacing between adjacent B875 chlorophylls found in natural systems.[2] The donor−acceptor distance varies between 24 Å near the center of the DNA duplex and 79 Å at the ends, as compared to a distance of 43 Å in the ringlike natural complex.[2]

Anchoring the complex to a lipid bilayer has two principal functions. First, it solubilizes the porphyrin, protecting it from the aqueous bulk solution. Second, and perhaps more interesting from a device perspective, it acts as a barrier allowing selective addressability of either the DNA in the aqueous phase or the porphyrin in the lipid phase. We have previously shown that porphyrin−DNA structures can be confined to a surface and still retain their chemical recognition properties, by binding the porphyrin into supported lipid bilayers.[27,28] Such a phase-separated system may also prove useful for harnessing the stored excitation energy.

As stated above, porphyrins are functional acceptors that are capable of partaking in redox reactions. Here we have chosen to use free-base porphyrin as the energy acceptor due to favorable photophysical properties. However, switching to the better reducing agent, zinc−porphyrin, only requires the addition of a few equivalents of $ZnCl_2$. The electron donor ability of excited zinc−porphyrins in DNA complexes similar to those studied here, have been previously demonstrated by using small electron-acceptor molecules which coordinate to the central zinc atom, culminating in the development of a bis-porphyrin binding pocket combining selective coordination of bidentate ligands with subsequent photoinduced ligand reduction.[29−31] In order to bind the ligands the porphyrin was situated in the hydrophobic environment of a liposome, thereby avoiding the competing coordination with water molecules.

YO was chosen as donor chromophore because it has a set of properties making it highly suitable for light-harvesting applications. It has a high absorption coefficient and fluorescence quantum yield when bound to DNA, yet it is virtually nonfluorescent in aqueous solution.[32,33] Further, energy transfer between YO dyes in close proximity is possible via a homo-FRET mechanism,[34] This property has been exploited for long-range excitation energy transfer from a donor via many intercalated YO to an acceptor over a distance of more than 20 nm.[3,35] Additionally, energy migration through networks of intercalated YO molecules has been shown to

dx.doi.org/10.1021/ja311828v | J. Am. Chem. Soc. 2013, 135, 2759−2768

selectively facilitate transfer of energy from a donor to a specific output acceptor.[36] YO and its homodimer YOYO have previously been used in the development of DNA-based nanotags for fluorescence microscopy, employing energy transfer to Cy3 acceptor dyes in a tetrahedral complex. This system displays many of the properties of photosynthetic light harvesting yet was not studied in this context.[37,38] Here, we wish to harness the homo-FRET possibilities provided by YO to shuttle excitation energy to the porphyrin over large distances, even from molecules at the ends of the DNA duplex, in a manner similar to that of the natural system, thereby effectively increasing the excitation of the porphyrin.

EXPERIMENTAL SECTION

A buffer consisting of 25 mM Tris HCl with 25 mM NaCl, adjusted to pH 8.0 using HCl was used for all experiments. Water was purified with a Milli-Q water purification system (Millipore, US).

Liposome Preparation. 1,2-Dioleoyl-*sn*-glycero-3-phosphocholine (DOPC) lipids were used for the formation of liposomes. Lipids, dissolved in chloroform, were purchased from Avanti Polar Lipids, US. Chloroform was removed using a rotavapor at low vacuum, followed by further drying at higher vacuum for >4 h, resulting in a dried lipid film. The dried film was rehydrated in buffer, followed by vortex mixing, subsequently 5 cycles of freezing in liquid N_2 and thawing at 35 °C. To form the liposomes the suspension was extruded 21 times through polycarbonate filters (Avestin, Canada, pore size 100 nm diameter). The final liposome stock concentration was ∼4 mg/mL. Mean liposome diameters were determined by dynamic light scattering using a Zetasizer Nano zs (Malvern, UK) at a lipid concentration of 0.016 mg/mL to be ∼120 nm, with a polydispersity index <0.1.

Characteristics of the DNA samples. Unmodified oligonucleotides were purchased (ATDBio,UK), and used without further preparation. Porphyrin modified oligomers were synthesized as described previously.[29] For the wire configuration, 39-mer duplex DNA was formed by mixing of two complementary strands, one containing a porphyrin modification, the other unmodified. A reference sample was also formed without porphyrin modification. The linker between the DNA and porphyrin was either two (**bipe**) or three (**tripe**) phenylethynylene units in length. The sequences of single strands used are shown in table 1. Double stranded porphyrin

Table 1. Single Strand Sequences Used to Create Wire Structures

strand	sequence	modification
bipe	5′-GGC CGC AAT CCC AAC CAA T*CA GCT AGA CAC ACT CAG ACG-3′	T* = bipe
tripe	5′-GGC CGC AAT CCC AAC CAA T*CA GCT AGA CAC ACT CAG ACG-3′	T* = tripe
DNA1	5′-GGC CGC AAT CCC AAC CAA TCA GCT AGA CAC ACT CAG ACG-3′	none
cDNA1	5′-CGT CTG AGT GTG TCT AGC TGA TTG GTT GGG ATT GCG GCC-3′	none

modified samples were prepared with a 1:1 ratio of complementary strands and 4× excess of EDTA (to remove Zn^{2+} left over from the synthesis), heated to 80 °C, and then annealed by slow cooling to room temperature overnight. The same procedure was used for unmodified duplexes, without the addition of EDTA.

Hexagonal DNA structures were designed on the basis of sequences from previous work.[28] The sequences are shown in the Supporting Information. The porphyrin moiety is identical to that used in sequence **tripe** in table 1.

DNA single strand concentrations were set prior to mixing using either DNA absorption at 260 nm for unmodified strands (ε_{cDNA1} = 361600 M^{-1} cm^{-1}, ε_{DNA1} = 375300 M^{-1} cm^{-1}) or free-base porphyrin absorption at 510 nm for porphyrin-labeled strands ($\varepsilon_{bipe/tripe}$ = 22000 M^{-1} cm^{-1}).

Labeling of **bipe** with the porphyrin moiety was incomplete during synthesis, and duplexes of this sequence were not included in steady-state measurements. For time-resolved measurements, the population showing a fluorescence lifetime corresponding to YO not quenched by FRET can be removed from the analysis. The incomplete labeling will therefore have little effect on the final result.

Formation of the Final Structures. To form the final wire complexes, DNA duplexes at 150 nM, liposomes at 150 mM lipid concentration and YO (at a given mixing ratio) were mixed and left overnight at room temperature to allow the porphyrin to bind to the bilayer, and the YOs to distribute randomly. For the highest YO:DNA mixing ratio DNA-porphyrin duplexes and liposomes were made at half concentration, to avoid a YO absorbance above 0.1. Hexagon structures were prepared similarly to the wire construct at 140 nM construct, 140 nM liposomes, at a given YO:porphyrin mixing ratio, and left overnight at 4 °C in a refrigerator. Dilutions were made in order to keep the YO absorbance below 0.1. Measurements were performed at room temperature for the wire constructs, and 5 °C for the hexagon construct. The lower temperature for the hexagon constructs was needed to stabilize the DNA duplex at the low salt concentrations needed for efficient intercalation of YO into the DNA.

Steady-State Optical Spectroscopy. Absorption measurements were performed on a Varian Cary 4000 or 5000 (Varian, US) instrument and data collected between 800 and 200 nm for all samples. Fluorescence excitation and emission spectra were collected using a Spex Fluorolog tau 3 spectrofluorimeter (Horiba, Japan). Corrected fluorescence emission spectra were collected between 490 and 800 nm, with excitation at 483 nm. Corrected fluorescence excitation spectra were collected between 480 and 600 nm, with emission monitored at 700 nm.

Time-Resolved Optical Spectroscopy. Time-resolved fluorescence measurements were performed on the 39-mer wire construct using time correlated single photon counting (TCSPC). The excitation pulse was provided by a Tsunami Ti:Sapphire laser (Spectra-Physics), pumped by a Millennia Pro X (Spectra-Physics). The 966 nm output was selected from the Tsunami, and the fundamental 82 MHz repetition rate was reduced to 4 MHz using a pulse picker. Finally, a 483 nm excitation pulse was obtained by second harmonic generation in a GWU-FHG (Spectra-Physics). The emitted photons were collected by a thermoelectrically cooled microchannel plate photomultiplier tube (R3809U-50, Hamamatsu). The signal was digitalized using a multichannel analyzer with 4096 channels (SPC-300, Edinburgh Analytical Instruments). Emission was recorded at 510 nm. Fluorescence decay curves of the samples containing only DNA and YO-PRO-1 were then fitted to two-exponential expressions by the program FluoFit Pro v.4 (PicoQuant GmbH). The obtained lifetimes and amplitudes were used as input parameters for fitting of the YO fluorescence decay in DNA−YO−porphyrin samples (both **bipe** and **tripe**) using an apparent distance distribution, implemented using a homemade Matlab routine (see Supporting Information).

RESULTS AND DISCUSSION

To improve the function of artificial light-harvesting complexes, rational design of the complete system is necessary, requiring a detailed mechanistic understanding of the parameters that affect light harvesting. In addition, a robust measure of system efficiency is needed, allowing a comparison between any light-harvesting systems. A suitable measure would need to be directly related to the number of excitation energy quanta transferred from donors to acceptor. Here we first present different ways to measure system performance before evaluating the performance of our model one-dimensional (1-D) 39 base-pair (bp) DNA−porphyrin wire system and discussing the mechanism behind the light-harvesting process. We then employ a Markov chain simulation to evaluate the effect of DNA wire length on system efficiency. On the basis of the results from the simulation a larger 99 bp two-dimensional

dx.doi.org/10.1021/ja311828v | J. Am. Chem. Soc. 2013, 135, 2759−2768

(2-D) DNA pseudohexagon structure is finally studied, showing a significant increase in harvested energy.

Measurement of System Efficiency. Generally, either the overall (energy) transfer efficiency (E) or a parameter coined the antenna effect (AE)[14] has been used to evaluate the efficiency of light-harvesting systems. Yet, it is important to clarify that neither measure alone is sufficient for the comparison of light-harvesting efficiency between different systems. E is the ratio between the number of excitation energy quanta transferred to the acceptor and the number of photons absorbed by the donors and thus describes the system after the initial excitation of donors. For a single-donor/single-acceptor system E is easily calculated from Förster theory (eqs 1 and 2).[39]

$$E = \frac{\frac{3}{2}\kappa^2\left(R_0^{DA}\right)^6}{\frac{3}{2}\kappa^2\left(R_0^{DA}\right)^6 + R^6} \tag{1}$$

$$R_0^{DA} = 0.197(n^{-4}QY_D \cdot J(\lambda))^{1/6} \tag{2}$$

In the above equations κ is the orientation factor between donor and acceptor transition dipole moments, R_0^{DA} is the dynamically averaged Förster radius at which energy transfer from donor to acceptor has a 50% probability, R is the donor–acceptor distance, n is the refractive index, QY_D is the donor quantum yield, and $J(\lambda)$ is the integrated spectral overlap of normalized donor fluorescence and acceptor absorption coefficient. For more complex systems with several donors, such as those studied here, all possible transfers from the donors must be considered. If donor fluorescence and absorption spectra overlap, the donors are able to transfer energy between themselves acting as both energy donor and acceptor (homo-FRET) which may in turn affect the overall transfer efficiency to the final acceptor (see below). For homo-FRET there is an associated spectral overlap and Förster radius, R_0^{DD}, which will differ from those pertaining to transfer from donor to final acceptor. The overall transfer efficiency does not take into account the absorption properties of the donors, a parameter which greatly influences the total number of excitation energy quanta reaching the acceptor, making it a poor general measure of system efficacy. If the donor absorption is low or there are few donors, even high E will not result in many excitation energy quanta reaching the acceptor, since the initial population of excited donors is low. The antenna effect has been used to remedy the lack of donor properties found in the overall transfer efficiency,[15,40,41] and is defined as the ratio between acceptor fluorescence when exciting the donors, to acceptor fluorescence upon direct excitation of the acceptor (i.e., no energy transfer, eq 3). However, this measure does not scale with the number of excitation energy quanta transferred from donor to acceptor and should therefore only be used when comparing systems employing the same acceptor.

$$AE = \frac{I_{A(ex,D)}}{I_{A(ex,A)}} = \frac{n_D \cdot \varepsilon_D \cdot E}{n_A \cdot \varepsilon_A} \tag{3}$$

In this expression, $I_{A(ex,D)}$ is the intensity of acceptor emission when exciting the donors, $I_{A(ex,A)}$ is the acceptor emission upon direct excitation of the acceptor, n_D is the number of donors, ε_D is the maximum absorption coefficient of the donor, n_A is the number of acceptors, ε_A is the maximum absorption coefficient of the acceptor, and E is the overall transfer efficiency from donors to acceptor. Equation 3 is best understood by considering its constituent parts; $n_D \cdot \varepsilon_D$ is directly related to the number of photons absorbed by the donors, multiplication by E yields the number of excitation energy quanta reaching the acceptor, division by n_A normalizes to the number of acceptors, yet the division by ε_A only serves as a further normalization factor. Generally, if ε_A is low, an inflated antenna effect is observed, since changes in R_0^{DA} (and hence changes in E) are not linear with respect to acceptor absorption coefficient. By multiplying eq 3 by ε_A, a relevant measure of the efficiency of light-harvesting systems is obtained, termed the effective absorption coefficient, ε_{eff} (eq 4). The effective absorption coefficient is directly proportional to the number of excitation energy quanta reaching the acceptor through energy transfer, and can be compared between different systems, employing different donors and acceptors.

$$\varepsilon_{eff} = AE \cdot \varepsilon_A = \frac{n_D \cdot \varepsilon_D \cdot E}{n_A} \tag{4}$$

Light-Harvesting Properties. Figure 2 shows normalized steady-state absorption and fluorescence emission spectra of the donor and acceptor. The shaded overlap between donor fluorescence and absorption allows effective homo-FRET whereas the overlap between donor emission and acceptor absorption allows hetero-FRET (a schematic drawing is shown in Figure 2). The emission from the porphyrin acceptor (700 nm) is well separated from that of the YO donor (510 nm) allowing direct detection of the weak porphyrin emission signal.

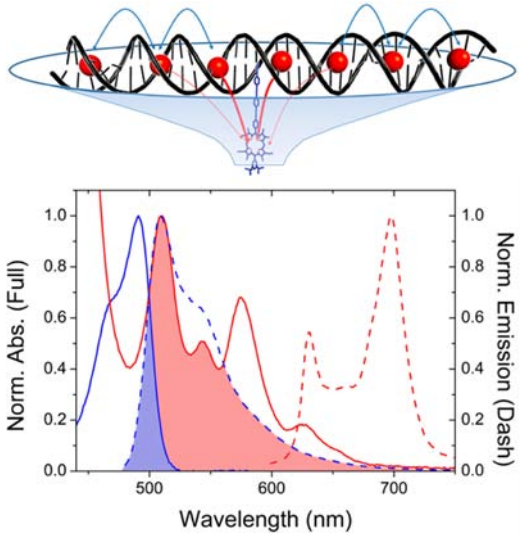

Figure 2. (Top) Schematic representation of the light-harvesting DNA–YO–porphyrin system. The red spheres represent intercalated YO molecules. The blue arrows show that homo-FRET between YO molecules funnels excitation energy toward the porphyrin, where hetero-FRET (red arrows) can occur. (Bottom) Normalized absorption (full lines) and fluorescence emission (dashed lines) spectra of YO and porphyrin, indicating the overlaps between fluorescence and absorption which allow hetero-FRET (red) and homo-FRET (blue).

To study the effect of YO concentration on the light-harvesting properties of the system, we varied the mixing ratio of YO:porphyrin between 2 and 20 at constant porphyrin–DNA concentration and performed steady-state fluorescence

dx.doi.org/10.1021/ja311828v | J. Am. Chem. Soc. 2013, 135, 2759–2768

measurements. The effective absorption coefficient and antenna effect are obtained from fluorescence excitation spectra, and the overall transfer efficiency is measured directly from donor quenching. These results are collected in Table 2.

Table 2. Light-Harvesting Properties as a Function of YO:Porphyrin Mixing Ratio

YO:porphyrin ratio	E^a	AE[b]	$\varepsilon_{eff} \times 10^3$ (M^{-1} cm^{-1})[c]
2	0.51 ± 0.03	2.2	48
5	0.51 ± 0.01	5.5	120
10	0.56 ± 0.02	8.9	200
20	0.49 ± 0.06	12	260

[a]Overall transfer efficiency. Standard deviations based on two measurements are shown. [b]Antenna effect. [c]Effective absorption coefficient.

Figure 3 shows fluorescence excitation spectra with increasing YO:porphyrin mixing ratios, measured at the

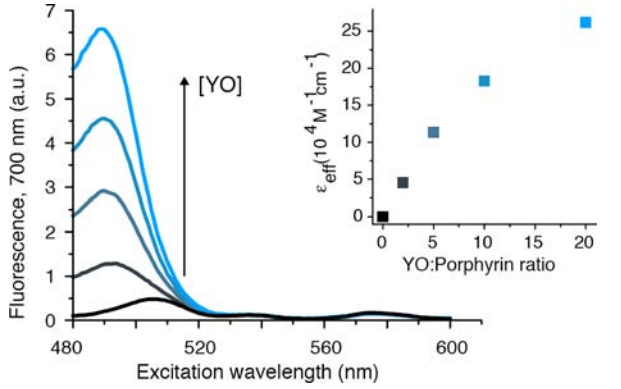

Figure 3. Fluorescence excitation spectra monitored at the porphyrin emission peak at 700 nm as a function of increasing YO:porphyrin ratio. The increase at 491 nm is due to an increase in the number of excitation energy quanta transferred from YO to porphyrin, due to the increase in YO concentration. (Inset) Calculated effective absorption coefficient of the porphyrin as a function of YO:porphyrin ratio.

porphyrin emission peak at 700 nm. The light-harvesting properties are clearly demonstrated as seen by the increase in acceptor fluorescence with increasing donor concentration upon exciting the donor absorption band between 480 and 520 nm. Absorption in the donor band increases with YO concentration, leading to increased porphyrin fluorescence through energy transfer from YO to porphyrin. The emission from YO is negligible in these measurements contributing only 5% of the signal (see Supporting Information). No change in the excitation spectrum is observed between 520 and 600 nm as only the porphyrin absorbs in this region, and the porphyrin concentration is unchanged at all mixing ratios. The effective absorption coefficient (inset in Figure 3) reaches 260000 M^{-1} cm^{-1} at the highest mixing ratio of 20:1, corresponding to a 31 times increase in absorbing power at this wavelength, and an antenna effect of 12. Increasing the YO concentration further to a mixing ratio of 40:1 had minimal effect on the antenna effect, and consequently minimal effect on ε_{eff}, indicating that the system is saturated with YO already at the mixing ratio of 20:1.

Effect of Homo-FRET on Overall Transfer Efficiency. To better understand the migration of energy after the initial excitation of a donor, the overall transfer efficiency was obtained from fluorescence emission spectra at each mixing ratio (Figure 4). The effect of energy transfer is clearly observed by a decrease in YO fluorescence and concomitant increase in

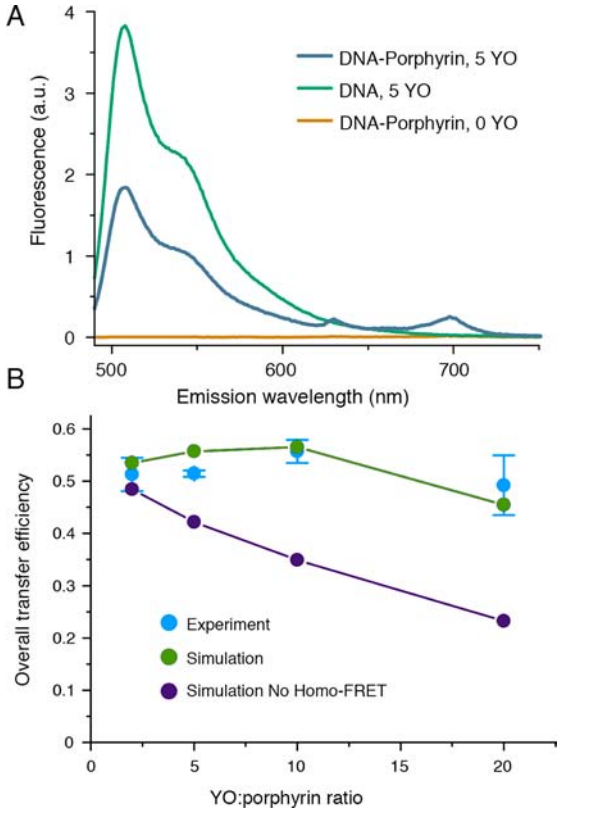

Figure 4. (A) Fluorescence emission of the porphyrin–DNA and DNA only systems at a mixing ratio of 5:1 (YO:porphyrin). The YO peak decreases when porphyrin is present due to energy transfer from YO to porphyrin. An increase in porphyrin emission is also observed. (B) Overall transfer efficiency as a function of YO:porphyrin mixing ratio for experimental and simulated data. The simulation is done both with and without the possibility of homo-FRET. The experimental data and simulated data with homo-FRET are in close agreement. The discrepancy between the two simulations increases as the YO:porphyrin ratio increases, reflecting that the influence from homo-FRET increases with YO concentration in the DNA wire.

porphyrin fluorescence when going from a donor-only to a donor–acceptor system at the mixing ratio of 5:1 (Figure 4A). To demonstrate the versatility of the system an experiment was performed using zinc–porphyrin instead of free-base porphyrin. The calculated R_0^{DA} values are nearly identical, and the measured overall transfer efficiency is also similar as expected (data not shown). The measured overall transfer efficiency is shown in Figure 4B (cyan circles) and is relatively constant (~55%) over the whole range of mixing ratios. This result may seem surprising at first, as an increase in YO concentration decreases the mean YO-to-YO distance and thereby increases the probability of homo-FRET transfers (eq 1), allowing the energy to migrate to a YO molecule positioned close enough to the porphyrin for hetero-FRET to occur. However, for YO the situation is complicated by changes in the photophysical properties of the dye as a function of the YO:DNA ratio; both the quantum yield and the lifetime of YO decrease as the concentration of intercalators within a DNA strand increases (see Supporting Information).[42] The change is quite severe, going from a quantum yield of 0.42 at the lowest binding ratio and dropping to 0.20 near saturation. Let us first examine the

dx.doi.org/10.1021/ja311828v | J. Am. Chem. Soc. 2013, 135, 2759–2768

system without taking into account the changes in YO photophysical properties. Consider the case with only a single YO bound to the DNA, furthest away from the porphyrin; the probability of transfer is governed by R_0^{DA} (~ 42 Å for the donor−acceptor pair at low YO concentration) which is much smaller than the actual distance between donor and acceptor (~ 79 Å). In this case the probability of hetero-FRET is near zero. Now consider the case where the DNA is saturated with YO, again with excitation occurring furthest from the acceptor; there is now a probability of a series of homo-FRET transfers ending at a YO molecule which is in close enough proximity to the acceptor for transfer to occur. In this case the probability of hetero-FRET is nonzero, since the energy has been transferred from the distal position to a position closer to the porphyrin. Now let us examine the effect of changes in YO photophysical properties. The quantum yield decrease lowers both R_0^{DA} and R_0^{DD} (eq 2), which means that the probability of transfer between two given molecules at a specific distance from each other decreases as more YO is added to the system. For homo-FRET the increased transfer due to a decrease in mean YO−YO separation outweighs the negative effect caused by the decrease in R_0^{DD}, meaning that homo-FRET will increase as a function of YO concentration. The near constant overall transfer efficiency as a function of YO concentration can then be explained by an increase in homo-FRET which increases E and a concomitant decrease in R_0^{DA}, which decreases E.

To corroborate the interpretation that the constant overall transfer efficiency stems from increased homo-FRET and simultaneous decrease in R_0^{DA}, we performed simulations of the overall transfer efficiency as a function of YO:porphyrin mixing ratio. A constant simulated overall transfer efficiency is observed, accurately reproducing the trend seen in the experimental results (Figure 4B green circles), supporting the above interpretation. The simulations are based on a Markov chain model which has previously been used to model the fluorescence depolarization for intercalated YO-to-YO energy transfer (see Supporting Information for a detailed description).[34] The simulation evaluates the probability of transferring excited state energy to the acceptor upon excitation of a single random donor at a certain donor:acceptor mixing ratio. The simulation is repeated 10000 times at each mixing ratio, using a random distribution of donors for each simulation cycle. In the simulation, solely the structure of B-DNA (which yields the relative distances and orientations between donors), the position of the acceptor, and experimental values for the Förster radii and YO lifetime as a function of YO:porphyrin mixing ratio are used as parameters. To investigate the effect of YO orientation on the simulated overall energy transfer efficiency, a second simulation was performed, assuming random orientation between donors. This yielded slightly higher transfer efficiency irrespective of mixing ratio, yet the difference between the two simulations was below 5%. To quantitatively estimate the contribution of energy transfer stemming from homo-FRET, we performed a third simulation where the probability of YO-to-YO transfer was set to zero (Figure 4B purple circles). At low YO concentrations, where homo-FRET is expected to be minimal due to large distances between adjacent YOs, the two simulations yield almost identical results. However, as the YO concentration increases, the difference between the two simulations becomes more prominent, culminating at saturation where homo-FRET effectively contributes to half of the transferred energy. This demonstrates an interesting approach where energy transfer simulations can be used to gain a better understanding of parameters that directly affect light harvesting.

In order to experimentally elucidate the influence of YO-to-YO resonance energy transfer on the light-harvesting behavior of the wire construct, the fluorescence decay of YO was studied using time correlated single photon counting. For this, two different linkers with varying lengths between the porphyrin and DNA were used, having either two or three phenylethynylene units. As there are multiple possible positions for YO to insert itself into the DNA, there are also multiple possible YO-to-porphyrin distances. Thus, the FRET process cannot be described by a single donor−acceptor distance; instead a distribution of distances, and hence also lifetimes, is required to provide an accurate representation of the system. Consider the case with a DNA−porphyrin assembly with only one intercalated YO molecule. As YO inserts randomly between the base-pairs along the strand, there will be an equal probability for all possible donor−acceptor distances (YO-to-porphyrin) in the system. In this case, the donor−acceptor distance is best characterized by a uniform distribution spanning all possible YO-to-porphyrin distances, ranging from the shortest distance at the base pair closest to the attachment point (24 Å and 18 Å for the long and the short linker, respectively) to the longest distance at the terminal base-pairs at either end of the DNA strand (~79 Å).

When more YO is added to the system, more sites fill up with intercalators. This means that the probability for YO-to-YO FRET will increase. Every intercalator in the system will experience the energy transfer landscape differently. For the intercalators positioned close to the porphyrin, the rate for energy transfer to the porphyrin will be significant. For the intercalators positioned toward the terminal base-pairs, the situation is the opposite. Here, probability for energy transfer to the porphyrin is low, and homo-FRET will dominate. The collective effect will be that lifetimes corresponding to short donor−acceptor distances become more heavily weighted, and lifetimes corresponding to long donor−acceptor distances will be diminished. As the excitation is moved closer to the porphyrin due to the influence of homo-FRET, a shift toward shorter distances is expected in the apparent distance distribution as the added amount of YO increases.

To qualitatively determine this experimentally we measured the fluorescence decay of YO at different YO:porphyrin ratios. The decay curves were fitted using an energy-transfer expression containing an apparent distance distribution rather than a single donor−acceptor distance, as shown in eq 5 (see Supporting Information for details). We have chosen to fit the decays using an apparent distance distribution, rather than directly using an equally valid lifetime distribution, for pedagogical reasons. Using an apparent distance distribution allows us to follow the effect of homo-FRET on the migration of energy along the wire as a function of intercalator density. The fitting algorithm was developed by Sandin et al.[43] and has later been used by Hannestad et al.[36]

$$I_{DA}(t) = g(t) \otimes \int_{R_{max}}^{R_{min}} \sum_i P(R)\alpha_i \times \exp[(-t/\tau_i)(1 + \{R/R_0^{DA}\}^6)]dR \quad (5)$$

Here, $g(t)$ is the instrument response function, R denotes the donor−acceptor distance, R_{min} and R_{max} are the minimum and maximum donor−acceptor separations, respectively, where $R_{min} = R_L$ (the linker length), $P(R)$ is the apparent distance

distribution function, α_i and τ_i are the intrinsic donor amplitudes and lifetimes, respectively (without the presence of acceptor), and R_0^{DA} is the Förster distance.

To represent the donor–acceptor distance distribution we use a 1-D Lorentzian distribution, eq 6, with the linker length as the center distance,

$$P(R) = \frac{2I}{\pi}\left[\frac{\gamma^2}{4(R - R_L)^2 + \gamma^2}\right] \quad (6)$$

where I and γ are the height and width of the distribution, respectively.

Figure 5 shows the results from the time-resolved fluorescence measurements. Both in the case of the assembly with a long linker (Figure 5A) and with a short linker (Figure 5B), the decay is best fitted with an almost uniform apparent distance distribution at two intercalators per strand. This indicates that each intercalator position along the DNA strand has an equal probability of being occupied, and each contributes a lifetime consistent with its distance to the porphyrin acceptor. . The uniform distribution does not mean that the energy-transfer efficiency is equal for every position, just that the excitation energy does not migrate from the YO molecule that originally absorbed it before energy transfer to the porphyrin occurs.

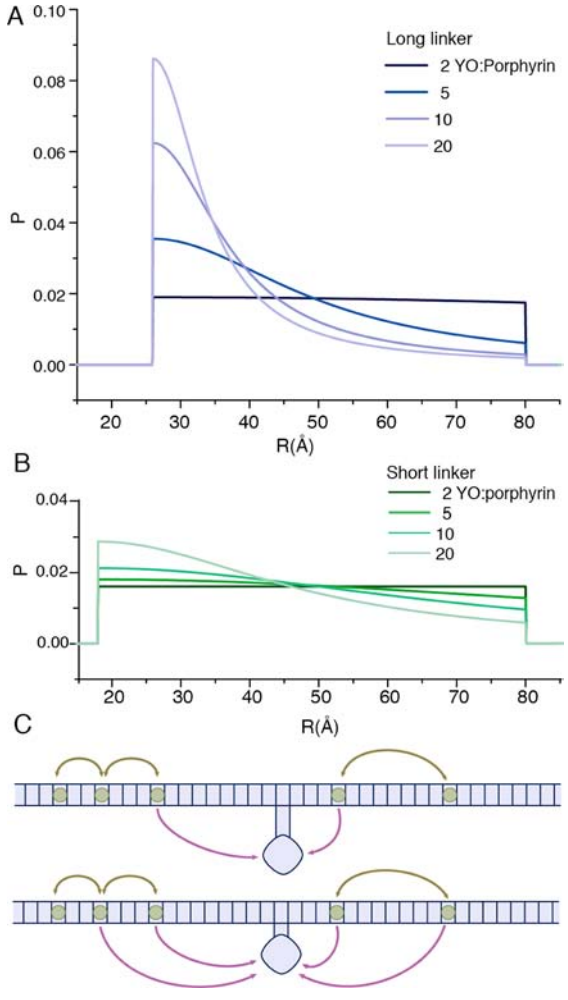

Figure 5. Apparent donor–acceptor distance distribution for DNA–porphyrin assembly shown as probability versus donor–acceptor distance, R with (A) long and (B) short linker at different YO concentrations. (C) Schematics of DNA–porphyrin–YO assemblies. The assembly with the short linker is more prone to direct energy transfer between YO and the porphyrin, while the system with the long linker relies on YO-to-YO homo-FRET for the excitation energy to reach the porphyrin.

When more YO is added to the system, there is an increased weight for the shorter distances, both for the long and for the short linker. This shows that, when the concentration of intercalator increases, the contribution of homo-FRET increases. Donor molecules far away from the porphyrin have transferred their energy to other donors instead of to the acceptor. The change in apparent distance distribution reflects a funneling of energy toward the acceptor as the donor concentration increases. Thus, we can conclude that, for a light-harvesting system comprising YO-PRO-1 and free-base porphyrins, energy transfer between individual YO molecules is an integral part of the light-harvesting effect, as was predicted from the Markov chain simulations.

Comparing the change in apparent distance distribution with YO concentration for the long and short linker it can be seen that the effect is more pronounced for the system with the long linker. The reason for this is highlighted in Figure 5C. In the system with the short linker, many more positions are within distance for direct energy transfer to the porphyrin, compared to the system with the long linker. Contrastingly, excitation energy located at intercalators distal from the porphyrin requires multistep energy transfer to reach the porphyrin. Because of this, the system with the long linker depends more on homotransfer than the system with the short linker and therefore also shows more pronounced changes in the apparent distance distribution with increased intercalator concentration.

In order to further investigate the extent of YO-to-YO homo-FRET in the system, we measured the fluorescence depolarization of samples containing only DNA and YO (no porphyrin) using time-resolved anisotropy. This technique has previously been used to study the unwinding of DNA upon intercalation.[44] When a single YO molecule bound to DNA is excited, its fluorescence depolarization is primarily due to rotational motion of the DNA molecule, which in the case of a 39 base-pair duplex is on the time scale of the fluorescence lifetime of YO.[45] However, if additional YO molecules are bound to the DNA within energy-transfer distance, the migration of the excitation energy will cause further depolarization of the emission. The effect of intercalator density on fluorescence depolarization has been described previously by Carlsson et al.[34] The results from the time-resolved anisotropy measurements at low YO densities show a 6.67 ns correlation time. As the YO concentration is increased, the correlation time decreases to 1.76 ns at 10 YO/strand and 0.66 ns at 20 YO/strand (see Supporting Information). Also the initial anisotropy decreases, from 0.2 at low YO density to 0.05 at 20 YO/strand. This large decrease indicates FRET processes which are faster than the time-resolution of the instrumentation. Such fast processes are expected due to homo-FRET between the closest spaced intercalators. As the density is increased, the mean YO-to-YO distance decreases, meaning that the fast FRET processes play a larger role, and the initial anisotropy will decrease with increasing YO density. The substantial decrease in the anisotropy further demonstrates that the YO–DNA system is characterized by extensive YO-to-YO FRET. Already at an average of two YO per strand the correlation time has decreased by 31%. The apparent energy

dx.doi.org/10.1021/ja311828v | J. Am. Chem. Soc. 2013, 135, 2759–2768

transfer distance distribution combined with the effect of energy transfer on the YO fluorescence anisotropy highlights the important role that energy transfer between identical intercalated YO molecules plays for the overall function of the light-harvesting assembly, meaning that dyes with small Stokes shift, allowing extensive homo-FRET, are preferable for the production of effective light-harvesting systems.

DNA Structure Design. In addition to investigating the influence of YO concentration on the overall transfer efficiency of the wire construct, we also used the Markov chain simulation to evaluate the effect of DNA wire length on the effective absorption coefficient (calculated as simulated overall transfer efficiency multiplied by both number of intercalated donors and donor absorption coefficient (eq 4)). This type of simulation can be used to find the optimal dimensions for maximal light harvesting. For short wire lengths high overall transfer efficiency is expected, since all donor molecules are in close proximity to the acceptor. However, if the wire is short, only a few donors are present, and the effective absorption coefficient may still be low, as seen in eq 4. Figure 6 shows simulated

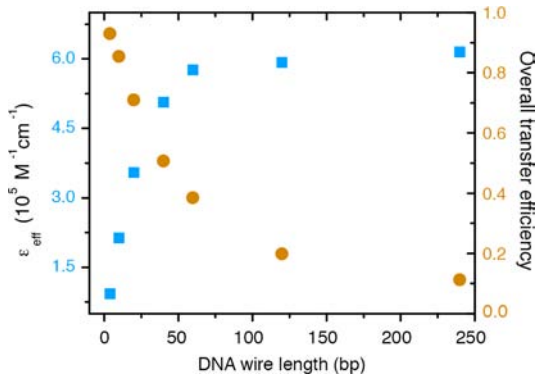

Figure 6. Simulated effective absorption coefficient (cyan squares) and simulated overall transfer efficiency (brown circles) as a function of DNA wire length, calculated using a YO density of 0.5 YO:bp (YO saturation density in DNA).

effective absorption coefficients and overall transfer efficiencies as a function of DNA wire length. As expected, the overall transfer efficiency is highest for the shortest DNA lengths, reaching 93% at 4 base-pairs. Interestingly, the effective absorption coefficient is lowest at this length and increases from 93000 M^{-1} cm^{-1} to a saturation value of ~600000 M^{-1} cm^{-1}, clearly demonstrating that sacrificing overall transfer efficiency can be useful if this is accompanied by a substantial increase in the number of donors. Saturation occurs near a wire length of 60 bp, indicating that there is not much to gain from our wire system by increasing the length of the DNA scaffold. To increase the effective absorption coefficient further we would need to expand into a second or third dimension by constructing branched DNA objects, in order to increase the number of donor molecules in proximity to the acceptor.

In order to investigate the effects of dimensionality, we constructed a 2-D light-harvesting assembly in the form of a pseudohexagon. The pseudohexagon consists of a 39 bp DNA duplex arm which connects to a duplex hexagon where each side is 10 bp long, yielding 99 base pairs in total. This means that roughly 50 YO molecules can bind to the structure, compared to the 20 YO which can bind to the wire at saturation. Each side of the hexagon is joined by a TT hinge, yielding a relatively flexible structure. The porphyrin acceptor is situated on the arm, nine bases away from the hexagon (see Figure 7). This yields a distance of ~102 Å from the porphyrin

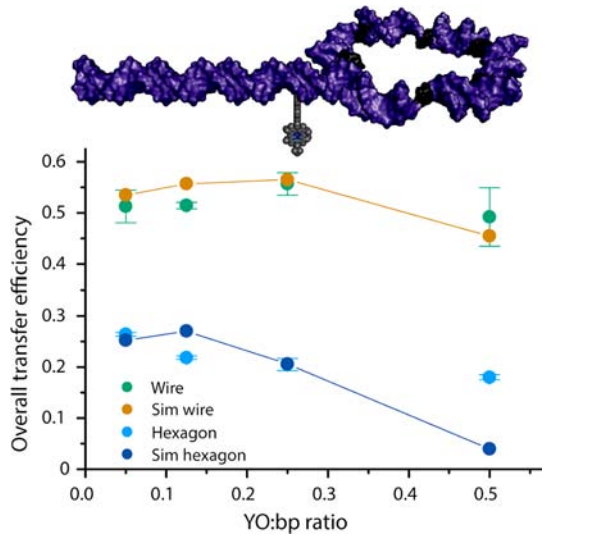

Figure 7. Experimental and simulated transfer efficiencies for the pseudohexagon structure. The experimental and simulated data for the wire are shown for comparison. A cartoon of the pseudohexagon DNA–porphyrin system is shown, where the flexible hinges (consisting of two unbase-paired thymines) are shown in black.

to the end of the arm, and ~102 Å from the porphyrin to the furthest part of the hexagon. The effect of dimensionality can be understood by considering the average donor–acceptor distance for the pseudohexagon versus a wire with an equal number of base-pairs. A 99 bp DNA wire saturated with intercalators will display an average distance between a donor and the acceptor of roughly 122 Å, whereas the value is reduced to 87 Å for the 99 bp pseudohexagon studied here. For the wire construct of 39 bp length described previously, the average distance is 48 Å. The light-harvesting properties were measured for this construct in the same way as for the DNA wire (see Supporting Information). Overall transfer efficiencies were generally lower for the hexagon (20–25%) as expected due to the larger distances between donors and acceptor (Figure 7). However, the effective absorption coefficient reaches 370000 M^{-1} cm^{-1} at saturation. This corresponds to an increase by a factor of 1.4 compared to the 39-mer wire. As with the wire construct the overall transfer efficiencies are constant over the whole range of mixing ratios. A simplified simulation of the overall transfer efficiency was performed (Figure 7 and Supporting Information). At low YO concentration the simulation and experimental data are in good agreement. As the concentration of YO is increased, the simulated overall transfer efficiency drops, whereas the measured efficiency remains constant. This can be explained by the flexibility of the structure, which is not included in the simulation. At low YO binding density, only YO molecules in close proximity to the porphyrin are involved in hetero-FRET energy transfer. The distances involved between these donors and the acceptor are not greatly influenced by the flexibility of the structure. When the structure is saturated with YO, donors far away from the porphyrin will be involved in the transfer of energy, meaning that flexibility plays a larger role in the transfer of excitation energy since it changes the relative positions of the dyes. The design of DNA–porphyrin light-harvesting structures presented

dx.doi.org/10.1021/ja311828v | J. Am. Chem. Soc. 2013, 135, 2759–2768

here is not limited to simple sticky-end DNA nanotechnology. One could apply the same principles to create more complex DNA scaffolds such as DNA origami. Furthermore, the approaches used here based on fluorescence measurements and Markov chain simulations are not limited to DNA or the dyes used. In principle any FRET-based light-harvesting complex can be studied in a similar manner.

CONCLUDING REMARKS

In this paper, we have presented a detailed study of the light-harvesting properties of novel DNA-based antenna complexes. The assembled structures showed efficient light-harvesting attaining an effective absorption coefficient of 260000 M^{-1} cm^{-1} for a 39-bp wire construct, and 370000 M^{-1} cm^{-1} for a larger, branched, pseudohexagon. This corresponds to an antenna effect of 12 and 17, respectively. By using components that self-assemble to form the final structure, it is possible to transfer the antenna complex design to more or less any DNA-based nanostructure. Further, we have shown, using both time-resolved fluorescence measurements and Markov chain simulations, how donor−donor energy transfer substantially contributes to the funneling of excitation energy to the porphyrin acceptor. The detailed understanding of the parameters which affect light harvesting will be crucial in the design of future light-harvesting complexes. For antenna systems to be efficient, it is important that they have a high donor:acceptor ratio. Having a donor capable of homo-FRET is therefore highly beneficial, as this allows the construction of larger systems, while retaining high overall transfer efficiency. Furthermore, the alternative strategy of organizing a series of donors and acceptors in a cascadelike fashion greatly increases the design complexity. More than being an acceptor, the porphyrin is also a lipid anchor that enables attachment not only to liposomes but also to supported lipid bilayers.[28] This platform can therefore be used for developing tools for surface-associated reactions where energy from light is used as a driving force in, e.g., molecular lithography. We envisage implementation of the design in more complex DNA assemblies where addressability allows positioning of multiple acceptors according to a predetermined pattern.[46,47]

ASSOCIATED CONTENT

Supporting Information

Light-harvesting properties of pseudohexagon, antenna effect calculation, Markov chain model, energy transfer distance distribution, YO time-resolved fluorescence anisotropy, pseudohexagon DNA strands. This material is available free of charge via the Internet at http://pubs.acs.org.

AUTHOR INFORMATION

Corresponding Author

balb@chalmers.se

Notes

The authors declare no competing financial interest.

ACKNOWLEDGMENTS

This research is funded by The Swedish Research Council (VR) and through the VR Linnaeus program SUPRA.

REFERENCES

(1) Hu, X. C.; Schulten, K. *Phys. Today* **1997**, *50*, 28−34.
(2) Hu, X. C.; Damjanovic, A.; Ritz, T.; Schulten, K. *Proc. Natl. Acad. Sci. U.S.A.* **1998**, *95*, 5935−5941.
(3) Su, W.; Schuster, M.; Bagshaw, C. R.; Rant, U.; Burley, G. A. *Angew. Chem., Int. Ed.* **2011**, *50*, 2712−2715.
(4) Schwartz, E.; Le Gac, S.; Cornelissen, J. J. L. M.; Nolte, R. J. M.; Rowan, A. E. *Chem. Soc. Rev.* **2010**, *39*, 1576−1599.
(5) Ziessel, R.; Harriman, A. *Chem. Commun.* **2011**, *47*, 611−631.
(6) Albinsson, B.; Hannestad, J. K.; Börjesson, K. *Coord. Chem. Rev.* **2012**, *256*, 2399−2413.
(7) Moore, T. A.; Gust, D.; Mathis, P.; Mialocq, J. C.; Chachaty, C.; Bensasson, R. V.; Land, E. J.; Doizi, D.; Liddell, P. A.; Lehman, W. R.; Nemeth, G. A.; Moore, A. L. *Nature* **1984**, *307*, 630−632.
(8) Steinberg-Yfrach, G.; Liddell, P. A.; Hung, S. C.; Moore, A. L.; Gust, D.; Moore, T. A. *Nature* **1997**, *385*, 239−241.
(9) Kuciauskas, D.; Liddell, P. A.; Lin, S.; Johnson, T. E.; Weghorn, S. J.; Lindsey, J. S.; Moore, A. L.; Moore, T. A.; Gust, D. *J. Am. Chem. Soc.* **1999**, *121*, 8604−8614.
(10) Gust, D.; Moore, T. A.; Moore, A. L. *Acc. Chem. Res.* **1993**, *26*, 198−205.
(11) Gust, D.; Moore, T. A.; Moore, A. L. *Acc. Chem. Res.* **2001**, *34*, 40−48.
(12) Iehl, J.; Nierengarten, J.-F.; Harriman, A.; Bura, T.; Ziessel, R. *J. Am. Chem. Soc.* **2012**, *134*, 988−998.
(13) Adronov, A.; Frechet, J. M. J. *Chem. Commun.* **2000**, 1701−1710.
(14) Brousmiche, D. W.; Serin, J. M.; Frechet, J. M. J.; He, G. S.; Lin, T. C.; Chung, S. J.; Prasad, P. N.; Kannan, R.; Tan, L. S. *J. Phys. Chem. B* **2004**, *108*, 8592−8600.
(15) Miller, R. A.; Presley, A. D.; Francis, M. B. *J. Am. Chem. Soc.* **2007**, *129*, 3104−3109.
(16) Dutta, P. K.; Varghese, R.; Nangreave, J.; Lin, S.; Yan, H.; Liu, Y. *J. Am. Chem. Soc.* **2011**, *133*, 11985−11993.
(17) Garo, F.; Häner, R. *Angew. Chem., Int. Ed.* **2012**, *51*, 916−919.
(18) Sessler, J. L.; Wang, B.; Harriman, A. *J. Am. Chem. Soc.* **1995**, *117*, 704−714.
(19) Seeman, N. C. *Nature* **2003**, *421*, 427−431.
(20) Seeman, N. C. *Nano Lett.* **2010**, *10*, 1971−1978.
(21) Pinheiro, A. V.; Han, D.; Shih, W. M.; Yan, H. *Nat. Nanotechnol.* **2011**, *6*, 763−772.
(22) Teo, Y. N.; Kool, E. T. *Chem. Rev.* **2012**, *112*, 4221−4245.
(23) Su, W.; Bonnard, V.; Burley, G. A. *Chem.—Eur. J.* **2011**, *17*, 7982−7991.
(24) Heilemann, M.; Tinnefeld, P.; Mosteiro, G. S.; Garcia-Parajo, M.; Van Hulst, N. F.; Sauer, M. *J. Am. Chem. Soc.* **2004**, *126*, 6514−6515.
(25) Albinsson, B. *Nature Chem.* **2011**, *3*, 269−270.
(26) Clegg, R. M.; Murchie, A. I. H.; Zechel, A.; Lilley, D. M. J. *Proc. Natl. Acad. Sci. U.S.A.* **1993**, *90*, 2994−2998.
(27) Woller, J. G.; Börjesson, K.; Svedhem, S.; Albinsson, B. *Langmuir* **2011**, *28*, 1944−1953.
(28) Börjesson, K.; Lundberg, E. P.; Woller, J. G.; Nordén, B.; Albinsson, B. *Angew. Chem., Int. Ed.* **2011**, *50*, 8312−8315.
(29) Börjesson, K.; Wiberg, J.; El-Sagheer, A. H.; Ljungdahl, T.; Mårtensson, J.; Brown, T.; Nordén, B.; Albinsson, B. *ACS Nano* **2010**, *4*, 5037−5046.
(30) Börjesson, K.; Woller, J. G.; Parsa, E.; Mårtensson, J.; Albinsson, B. *Chem. Commun.* **2012**, *48*, 1793−1795.
(31) Börjesson, K.; Tumpane, J.; Ljungdahl, T.; Wilhelmsson, L. M.; Nordén, B.; Brown, T.; Mårtensson, J.; Albinsson, B. *J. Am. Chem. Soc.* **2009**, *131*, 2831−2839.
(32) Carlsson, C.; Larsson, A.; Jonsson, M.; Albinsson, B.; Nordén, B. *J. Phys. Chem.* **1994**, *98*, 10313−10321.
(33) Larsson, A.; Carlsson, C.; Jonsson, M.; Albinsson, B. *J. Am. Chem. Soc.* **1994**, *116*, 8459−8465.
(34) Carlsson, C. L., A.; Björkman, M.; Jonsson, M.; Albinsson, B. *Biopolymers* **1997**, *41*, 481−494.
(35) Hannestad, J. K.; Sandin, P.; Albinsson, B. *J. Am. Chem. Soc.* **2008**, *130*, 15889−15895.

(36) Hannestad, J. K.; Gerrard, S. R.; Brown, T.; Albinsson, B. *Small* **2011**, *7*, 3178−3185.
(37) Benvin, A. L.; Creeger, Y.; Fisher, G. W.; Ballou, B.; Waggoner, A. S.; Armitage, B. A. *J. Am. Chem. Soc.* **2007**, *129*, 2025−2034.
(38) Özhalıcı-Ünal, H.; Armitage, B. A. *ACS Nano* **2009**, *3*, 425−433.
(39) Lakowicz, J. R., *Principles of Fluorescence Spectroscopy*, 3rd ed.; Springer: New York, 2006.
(40) Brousmiche, D. W.; Serin, J. M.; Frechet, J. M. J.; He, G. S.; Lin, T. C.; Chung, S. J.; Prasad, P. N.; Kannan, R.; Tan, L. S. *J. Phys. Chem. B* **2004**, *108*, 8592−8600.
(41) Dutta, P. K.; Varghese, R.; Nangreave, J.; Lin, S.; Yan, H.; Liu, Y. *J. Am. Chem. Soc.* **2011**, *133*, 11985−11993.
(42) Larsson, A.; Carlsson, C.; Jonsson, M. *Biopolymers* **1995**, *36*, 153−167.
(43) Sandin, P.; Lincoln, P.; Albinsson, B. *J. Phys. Chem. C* **2008**, *112*, 13089−13094.
(44) Tichadou, J. L.; Genest, D.; Wahl, P.; Aubelsadron, G. *Biophys. Chem.* **1975**, *3*, 142−146.
(45) Tirado, M. M.; Garciadelatorre, J. *J. Chem. Phys.* **1980**, *73*, 1986−1993.
(46) Voigt, N. V.; Torring, T.; Rotaru, A.; Jacobsen, M. F.; Ravnsbaek, J. B.; Subramani, R.; Mamdouh, W.; Kjems, J.; Mokhir, A.; Besenbacher, F.; Gothelf, K. V. *Nat. Nanotechnol.* **2010**, *5*, 200−203.
(47) Stein, I. H.; Steinhauer, C.; Tinnefeld, P. *J. Am. Chem. Soc.* **2011**, *133*, 4193−4195.